Laser and Particle Beams (2016), *34*, 433–439.

doi:10.1017/S0263034616000318

Photo-transmutation of long-lived radionuclide ^{135}Cs by laser–plasma driven electron source

X.-L. WANG,[1] Z.-Y. TAN,[1] W. LUO,[1,2] Z.-C. ZHU,[1] X.-D. WANG,[1] AND Y.-M. SONG[1]

[1]College of Nuclear Science and Technology, University of South China, 421001 Hengyang, China
[2]Extreme Light Infrastructure-Nuclear Physics, "Horia Hulubei" National Institute for Physics and Nuclear Engineering (IFIN-HH), 30 Reactorului, 077125 Bucharest-Magurele, Romania

(RECEIVED 5 November 2015; ACCEPTED 20 May 2016)

Abstract

Laser-driven relativistic electrons can be focused onto a high-*Z* convertor for generating high-brightness γ-rays, which in turn can be used to induce photonuclear reactions. In this work, photo-transmutation of long-lived radionuclide ^{135}Cs induced by laser–plasma–interaction-driven electron source is demonstrated using Geant4 simulation (Agostinelli *et al.*, 2003 *Nucl. Instrum. Meth. A* **506**, 250). High-energy electron generation, bremsstrahlung, as well as photonuclear reaction are observed at four different laser intensities: 10^{20}, 5×10^{20}, 10^{21}, and 5×10^{21} W/cm^2. The transmutation efficiency depends on the laser intensity and target size. An optimum laser intensity, namely 10^{21} W/cm^2, was found, with the corresponding photonuclear reaction yield reaching 10^8 J^{-1} of the laser energy. Laser-generated electrons can therefore be a promising tool for transmutation reactions. Potential application in nuclear waste management is suggested.

Keywords: Photo-transmutation; ^{135}Cs; Bremsstrahlung γ-rays; Nuclear waste; Laser ponderomotive acceleration

1. INTRODUCTION

Beams of electrons, positrons, protons, and high-energy photons can result from the interaction of ultra-intense lasers with solid or gas targets. The process has received much attention because of its many potential applications (Ledingham *et al.*, 2003; Mangles *et al.*, 2004; Schwoerer *et al.*, 2006; Luo *et al.*, 2013, 2015; Hanus *et al.*, 2014). Thanks to recent advances in laser technology, laser-driven electrons can be accelerated to hundreds MeVs. By focusing the resulting relativistic electrons onto a high-*Z* metallic target, high-energy γ-rays can be generated through bremsstrahlung. Such radiation has a wide range of applications, such as activation (or transmutation), fission, and fusion (Ledingham *et al.*, 2003; Schwoerer *et al.*, 2003; Galy *et al.*, 2007, 2009).

Photonuclear reaction induced by ultra-intense laser was first proposed by Shkolnikov *et al.* (1997), and bremsstrahlung γ-rays, positrons, and photoneutrons were obtained. Magill *et al.* (2003) performed a photo-transmutation experiment on the long-lived radionuclide ^{129}I to confirm the existing reaction cross-sections for ^{129}I (γ, *n*). Photo-transmutation of the radionuclides ^{135}Cs, ^{137}Cs, ^{90}Sr, ^{93}Zr, and ^{126}Sn driven by laser-based electron-bremsstrahlung have also been considered (Takashima *et al.*, 2005; Sadighi-bonabi & Kokabee, 2006; Sadighi & Sadighi-Bonabi, 2010; Sadighi-bonabi *et al.*, 2010; Irani *et al.*, 2012). These studies suggest that the number of photonuclear reactions is closely related to the laser intensity and irradiation time, and laser-based photo-transmutation of radioactive nuclear waste should be possible. However, these studies are limited to theoretical calculations for thin targets. They do not take into account γ-ray attenuation inside the targets, nor other reaction channels that can be competitive with the (γ, *n*) reactions. Furthermore, without considering the target geometry, transmutation of long-lived radionuclides cannot be optimized.

In this work, we report a proof-of-principle experiment on the transmutation of long-lived nuclear waste ^{135}Cs by ultra-intense laser with intensity $(0.1\text{–}5.0) \times 10^{21}$ W/cm^2. The radionuclide ^{135}Cs has high radiotoxicity, long half-life ($T_{1/2} = 2.3$ million years), as well as geologic repository impact and inventory, so that it risks leakage into the biosphere (Yang *et al.*, 2004). Using the photo-transmutation method, ^{135}Cs can be transmuted into ^{134}Cs through the (γ, *n*) reaction or into the stable nuclide ^{133}Cs through the (γ, 2*n*) reaction. The ^{134}Cs has a short half-life of 2.07 years as it beta decays into the stable nuclide ^{134}Ba. These non-/low toxic or stable product nuclides can be easily handled. Although the transmutation of ^{135}Cs by ultra-intense laser has been analytically demonstrated (Takashima *et al.*,

Address correspondence and reprint requests to: W. Luo, College of Nuclear Science and Technology, University of South China, 421001 Hengyang, China. E-mail: wenluo-ok@163.com

2005) earlier, the effect of the laser intensity and target geometry on the details of the transmutation reactions is still unexplored.

Here, a photo-transmutation model, together with the Geant4 toolkit (Agostinelli *et al.*, 2003), is developed for the transmutation of long-lived radionuclides using laser ponderomotive acceleration (LPA) of energetic electrons. In this model, the properties of the LPA produced electron beam (*e*-beam), such as the spectral and angular distributions, as well as competitive reaction channels that can result in additional contribution to the transmutation yield, are fully taken into account. Generation of intense bremsstrahlung γ-ray source driven by the laser-accelerated *e*-beam is investigated along with the photo-transmutation of ^{135}Cs. Attention is also given to the dependence of the transmutation yield on the geometry of the converting target (CT) for bremsstrahlung generation and the adjacent transmuted target (TT), such as to optimize the number of transmutation reactions. It will be helpful for the similar photonuclear experiments performed by using high-peak power lasers.

Our study shows that the transmutation reaction yield can be enhanced more than three times by using an optimized target geometry and considering the contribution of electrons escaped from the rear side of the CT. It can reach 10^8 J^{-1} of laser pulse energy. This makes transmutation of nuclear wastes using state-of-the-art lasers quite promising. It should be reminded warmly that these phenomena can hardly be revealed according to the previous calculations.

2. PHOTO-TRANSMUTATION MODEL

Currently, laser wakefield acceleration (LWFA) and LPA are the main table-top electron acceleration schemes (Esarey *et al.*, 2009). LWFA can deliver high-quality relativistic (≥100 MeV) *e*-beams with low (a few percent) energy spread and small (a few mrad) spatial divergence, but the beam current that can be accelerated is limited to tens pC. In contrast, LPA can generate relativistic *e*-beams up to a few nC (Glinec *et al.*, 2005; Giulietti *et al.*, 2008), which is useful for increasing the bremsstrahlung γ flux. Moreover, LPA *e*-beams have a wide bandwidth, and the need for narrowing their spectra is not needed since the bremsstrahlung γ source also has a continuous spectrum pattern. Accordingly, we shall use LPA *e*-beams to produce bremsstrahlung γ-rays, which in turn induce photo-transmutation of the cesium target.

A scheme for photo-transmutation of long-lived radionuclide ^{135}Cs by the LPA *e*-beam is illustrated schematically in Figure 1. Because of its relative high conversion efficiency and more acceptable price than the more efficient but expensive Au target (Yan *et al.*, 2012), metallic tantalum is used as the bremsstrahlung convertor. Both the convertor and the cesium target are assumed to have cylindrical structures with flexible radii and thicknesses. Since the dependence of the LPA *e*-beam spectra and angular distribution on the

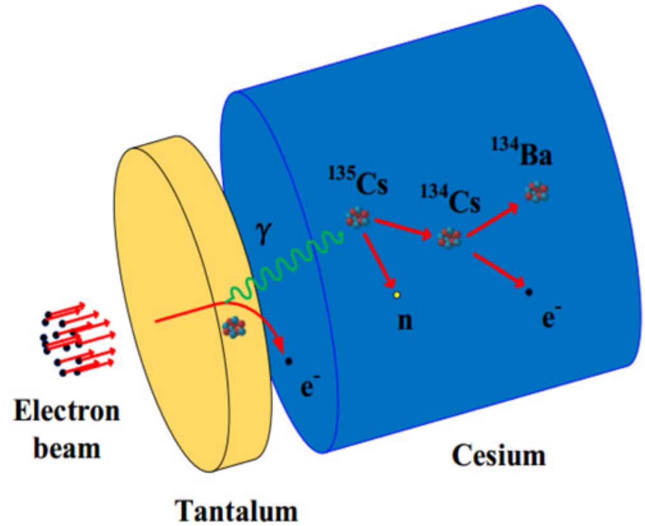

Fig. 1. Schematic diagram of the transmutation of radionuclide ^{135}Cs by laser-driven *e*-beam. For better visualization of the target structure, space has been added between the tantalum and cesium components.

laser intensity has been well characterized, we can implement directly in the Geant4 simulations the characteristics of the LPA *e*-beams for the incident laser intensities 10^{20}, 5×10^{20}, 10^{21}, and 5×10^{21} W/cm^2, with pulse energies 0.37, 1.86, 3.72, and 18.62 J, respectively and spot size 2.5 μm [full-width at half-maximum (FWHM)]. The laser-to-electrons energy conversion efficiency is fixed at 30%, achieved by selecting appropriate acceleration lengths (Sentoku *et al.*, 2002; Chen *et al.*, 2009; Tanimoto *et al.*, 2009; Hanus *et al.*, 2014). For the given energy conversion efficiency, the number of electrons can be related to the incident laser energy.

In order to reduce the computing time, a total of 10^8 electrons are used in the Geant4 simulations and they have a Maxwellian energy distribution (Tanimoto *et al.*, 2009; Antici *et al.*, 2012)

$$f(E) = \frac{2}{\sqrt{\pi} k T_h^{3/2}} \sqrt{E_e} \exp\left(-\frac{E_e}{T_h}\right), \quad (1)$$

where E_e is the kinematic energy of the LPA electrons, k is the Boltzmann constant and T_h is the electron temperature (Wilks *et al.*, 1992)

$$T_h = 0.511\left[\sqrt{\left(1 + \frac{I\lambda_\mu^2}{1.37}\right)} - 1\right] \quad (2)$$

where I is the laser intensity in W/cm^2 and λ_μ is the wavelength in μm. From Eq. (1) we can obtain the spectral distribution of the LPA *e*-beams for different laser intensities, as shown in Figure 2. We see that the laser intensity has an important effect on the *e*-beam spectrum: the higher the laser intensity, the larger the number of the energetic electrons. Thus, together with the cross-sections of photonuclear

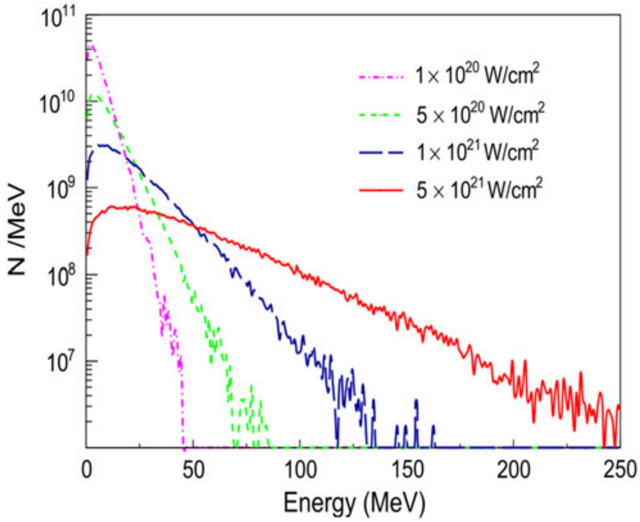

Fig. 2. Energy spectrum of LPA *e*-beams for the laser intensity varying from 10^{20} to 5×10^{21} W/cm^2.

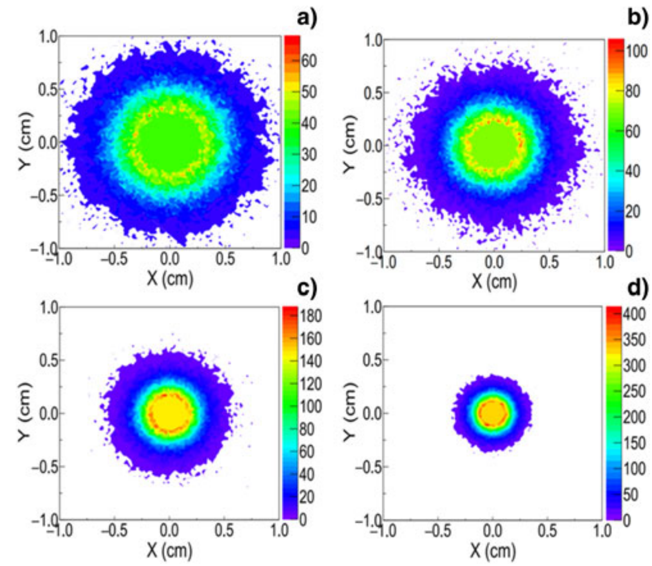

Fig. 3. The transverse distribution of the LPA *e*-beam recorded at 1 cm downstream of the initial position of the *e*-beam for the laser intensities 10^{20} W/cm^2 (a), 5×10^{20} W/cm^2 (b), 10^{21} W/cm^2 (c), and 5×10^{21} W/cm^2 (d).

reactions, one can optimize the number of reactions by varying the dimensions of the convertor and the cesium target, as discussed in Section 4.

An *e*-beam with spot size 3 μm (FWHM) impinges on the front surface of the convertor. It has a Gaussian energy distribution and angular spread (Moore *et al*., 1995; Quesnel & Mora, 1998; Debayle *et al*., 2010)

$$\theta = \tan^{-1}\sqrt{\frac{2}{(\gamma - 1)}}, \quad (3)$$

where γ is the Lorenz factor of the relativistic electrons. The transverse profile of the *e*-beam from Eq. (3) is shown in Figure 3. Such a profile was recorded at 1 cm downstream of the initial position of the *e*-beam. We see that the *e*-beams produced by higher intensity lasers are more collimated and have higher energy.

3. SECONDARY SOURCES DRIVEN BY LPA ELECTRON BEAM

In general, the reaction yield depends on the convolution of the bremsstrahlung spectrum and the cross-sections of the photonuclear reactions. The interaction of the LPA electrons (see Figs 2 and 3) with the convertor is simulated for the laser intensities 10^{20}, 5×10^{20}, 10^{21}, and 5×10^{21} W/cm^2, and secondary products such as electrons, positrons, and bremsstrahlung γ-rays are generated. Figure 4 shows the bremsstrahlung spectrum, produced by the LPA *e*-beam interacting with a 1.5 mm thick tantalum convertor. Also shown in Figure 4 is the total cross-sections of (γ, *n*) and (γ, 2*n*) reaction with ^{135}Cs. Competitive reactions such as (γ, 3*n*), (γ, α), (γ, *p*), (γ, *n* + *p*), (γ, *n* + α), and (*e*, *n*) are not included in the figure because their reaction cross-sections are below 10 mbarn. The transmutation reaction has neutron separation energy of 8 MeV, its peaked cross-section occurs at about 15 MeV. At laser intensities below 10^{21} W/cm^2, the photonuclear reaction yield caused by the bremsstrahlung γ-rays increases with the laser intensity according to the convolution between the bremsstrahlung spectrum and the reaction cross-section, as shown in Figure 4. However, at laser intensities above 10^{21} W/cm^2, the reaction yield increases slowly.

Together with the bremsstrahlung γ-rays from the rear face of the convertor, the emitted secondary electrons and positrons can also irradiate the TT and produce high-energy bremsstrahlung γ-rays, which in turn trigger additional photonuclear reactions. The resulting electron and the positron spectra are shown in Figure 5. The target dimension is the same as that in Figure 4. It is found that both the electron and positron beams have Maxwellian-like spectral distributions. The numbers of high-energy electrons and positrons increase with the laser intensity. Due to the overlap of the energy spectra with the reaction cross-sections (see Fig. 4), similar to the bremsstrahlung γ-rays they can contribute to the transmutation yield. However, since the positrons are relatively few compared with the electrons, their contribution can be neglected.

Considering that the γ-rays and electrons with energies below the neutron separation energy cannot induce the photonuclear reaction, at four different laser intensities we counted the yield of electrons and γ-rays with energies above 6 MeV, as shown in Figure 6. As the CT thickness is increased, the secondary electrons decrease, but the γ-rays increase and become saturated for the few-mm thick target. The γ-ray yield is of order 10^{10} J^{-1} (of laser energy). The peaked values 1.0×10^{10}, 1.8×10^{10}, 3.1×10^{10}, and 3.7×10^{10} J^{-1} are obtained for the CT thicknesses 1.5, 2.5, 3.5, and 5.5 mm, respectively. That is, as the laser intensity increases, the thickness of the convertor should be increased.

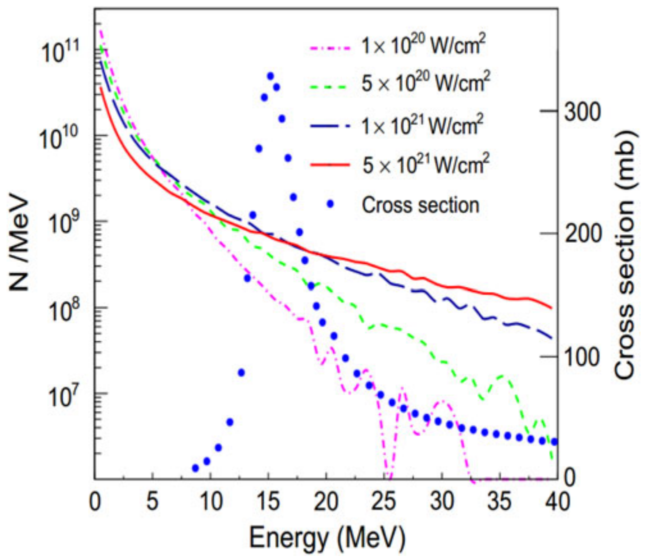

Fig. 4. The bremsstrahlung spectrum for four laser intensities, together with the total cross-sections of (γ, n) and (γ, $2n$) reactions with ^{135}Cs. The radius and the thickness of the CT in the simulation are $r_1 = 2$ cm and $T_1 = 1.5$ mm, respectively.

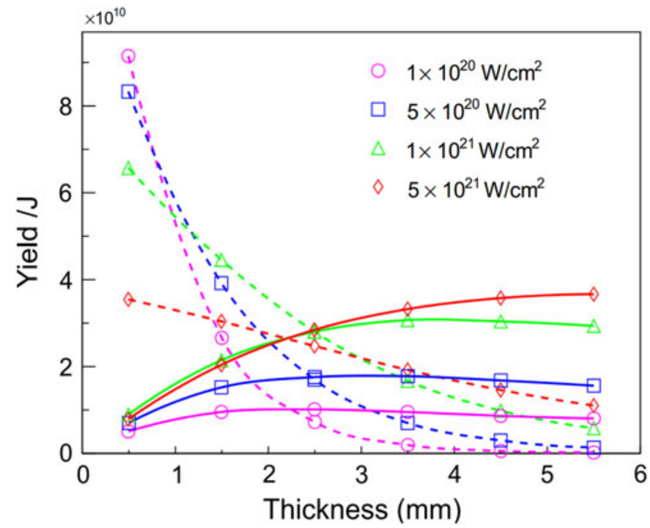

Fig. 6. The γ-ray (solid curves) and the electron (dashed curves) yields as a function of the CT thickness at laser intensities between 10^{20} and 5×10^{21} W/cm^2. γ-rays and electrons with the energies over 6 MeV are taken into account due to the neutron separation energy of 8 MeV. The radius of the convertor was fixed to be $r_1 = 2$ cm in the simulation.

4. PHOTO-TRANSMUTATION OF ^{135}CS

We now consider the influence of the target parameters on the transmutation yield of ^{135}Cs. We shall concentrate on the thickness of the convertor, the radius and thickness of the transmuted target, and the transmutation of ^{135}Cs resulting from the dominant (γ, n) and (γ, $2n$) reactions. It is found that other competitive reactions account for only 3% of the total product, so that they are neglected, even though the product nuclides such as ^{132}Cs, ^{131}I, ^{134}Xe, and ^{133}Xe are short-lived or stable. This can also be understood in terms of the reaction cross-sections, as discussed above.

4.1. The Influence of CT Thickness

The secondary sources driven by the LPA *e*-beam are used to transmute the long-lived nuclear waste ^{135}Cs. Figure 7 shows the contribution of the secondary particles to transmutation reactions together with the total contributions at different laser intensities. In the simulation, the radius of the CT is 2 cm, and the radius and thickness of the TT are 4 and 3 cm, respectively. For a thin CT, the electrons contribute much more to the transmutation reactions than the bremsstrahlung γ-rays. With increase of the CT thickness, the contribution of the electrons decreases but that of the γ-rays increases. However, as the CT thickness attains a certain value, the contribution of the γ-rays decreases because of their decreased yield. It is also shown in Figure 7 that due to the contribution of electrons the thickness of the CT that led to the maximum total reaction yield is slightly thinner than that led to the peak γ-ray yield. This suggests that the influence of the electrons should be taken into account in order to obtain reliable reaction yield. This effect has not been discussed in the existing literature. In addition, the contribution of the positrons is found to be much smaller than 7% and is thus not shown in the figure.

Figure 7 also shows the dependence of the total reaction yield on the CT thickness. As the value of the thickness of

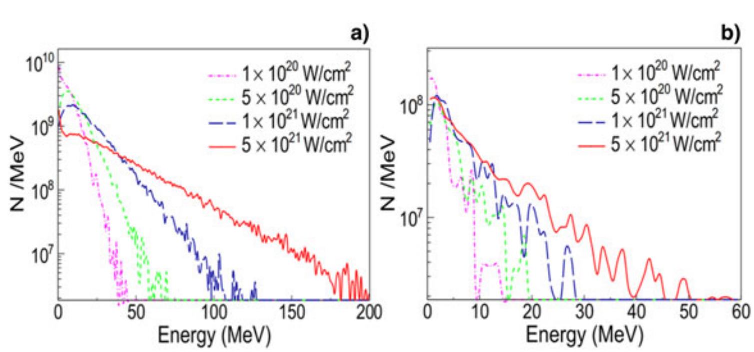

Fig. 5. The electron spectrum (a) and positron spectrum (b) for the laser intensity varying from 10^{20} to 5×10^{21} W/cm^2. The target geometries were chosen as the same as in Fig. 4.

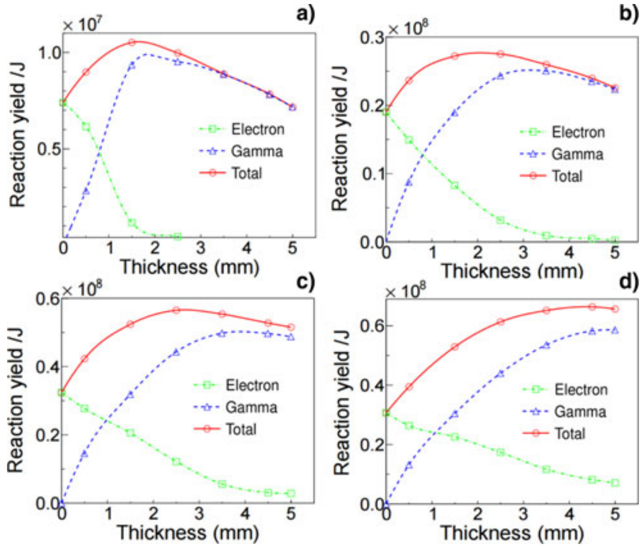

Fig. 7. The contribution of the electrons and bremsstrahlung γ-rays to the transmutation reaction at laser intensities of 10^{20} W/cm^2 (a), 5×10^{20} W/cm^2 (b), 10^{21} W/cm^2 (c), and 5×10^{21} W/cm^2 (d). The total contribution is also shown in the figure. The radius of the CT used in the simulations was $r_1 = 2$ cm, and the radius and thickness of the TT were $r_2 = 4$ cm and $T_2 = 3$ cm, respectively.

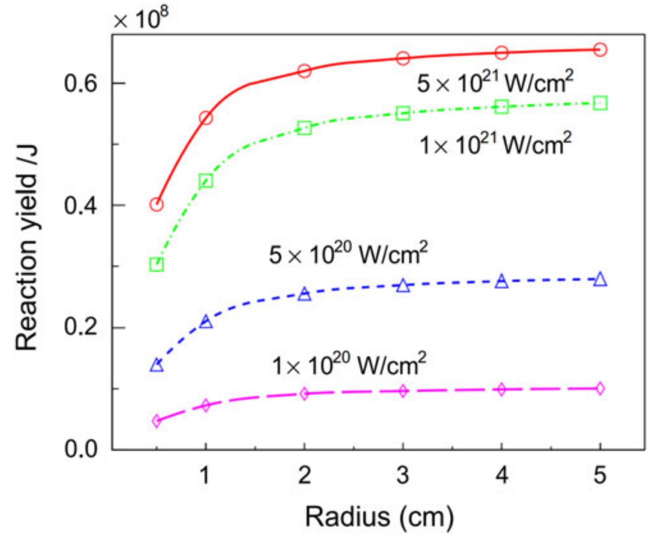

Fig. 8. The reaction yield as a function of the TT radius at laser intensities varying from 10^{20} to 5×10^{21} W/cm^2. While keeping the same values for the CT radius and the TT thickness as those used in Fig. 7, that is, $r_1 = 2$ cm, $T_2 = 3$ cm, we used the optimized convertor thickness as follows: $T_1 = 1.0$, 1.5, 2.5, and 3.5 mm at laser intensities of 10^{20}, 5×10^{20}, 10^{21}, and 5×10^{21} W/cm^2, respectively.

the CT is set to 0, it means the case of "without CT", from which the LPA *e*-beam irradiated on the transmuted target directly and then triggered the photonuclear reactions. One can see that with the help of the CT, the transmutation yield is enhanced. In order to obtain the maximum reaction yield, the optimized thickness for the CT is found to be 1.0, 1.5, 2.5, and 3.5 mm at laser intensities of 10^{20}, 5×10^{20}, 10^{21}, and 5×10^{21} W/cm^2, respectively. While the CT thickness below 1.5 mm, the reaction yield at laser intensity 5×10^{21} W/cm^2 (see Fig. 7d) is slightly smaller than that at 10^{21} W/cm^2 (see Fig. 7c). This is mainly caused by the convolution of the γ spectrum with the profile of the photonuclear cross-section, as discussed above.

4.2. Effect of the Geometry of the Transmuted Target

Using the optimized thickness of the CT, the dependence of transmutation reactions on the TT geometry was investigated. The curve of the reaction yield as a function of the TT radius is investigated and is shown in Figure 8. The reaction yield enhanced rapidly when the target radius is relatively small, for example, ≤1.0 cm, meanwhile such enhancement ceased when the radius of the target larges 1.5 cm. Taking into account the volume of the TT, the radius of the TT is suggested to be 2 cm at four different laser intensities. In the simulation, the thickness of the TT was set as 3 cm.

The dependence of the reaction yield on the TT thickness for different laser intensities is shown in Figure 9. The radii of the CT and TT are 2 cm, and the optimized thicknesses of the CT are used in the simulation, as discussed above. For ≥10^{21} W/cm^2 lasers, the reaction yield increases with the

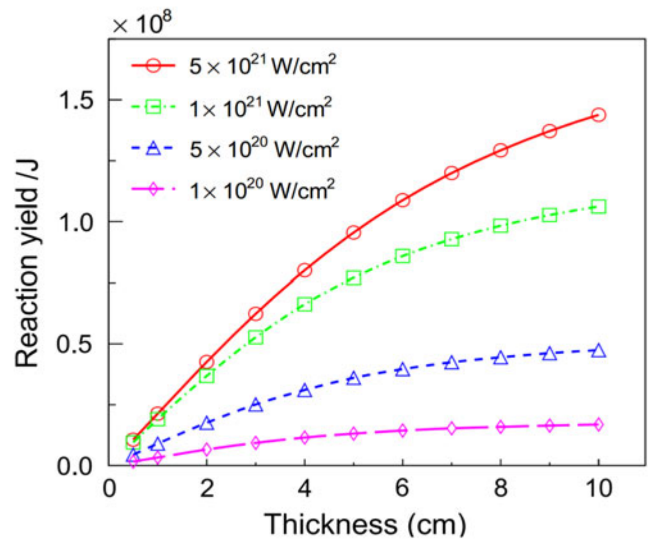

Fig. 9. The reaction yield versus TT thickness at different laser intensities. The optimized parameters of the targets used in the simulation are the following: $r_1 = 2$, $r_2 = 2$ cm, and $T_1 = 1.0$, 1.5, 2.5, and 3.5 mm at laser intensities of 10^{20}, 5×10^{20}, 10^{21}, and 5×10^{21} W/cm^2, respectively.

thickness of the TT. At the lower laser intensities, such increase is not obvious or even absent.

4.3. Discussion

At laser intensities ranging from 10^{20} to 5×10^{21} W/cm^2, the influence of the parameters for both the convertor and transmuted target has been demonstrated (see Figs 7–9). According to these simulations, the transmutation yield of ^{135}Cs was

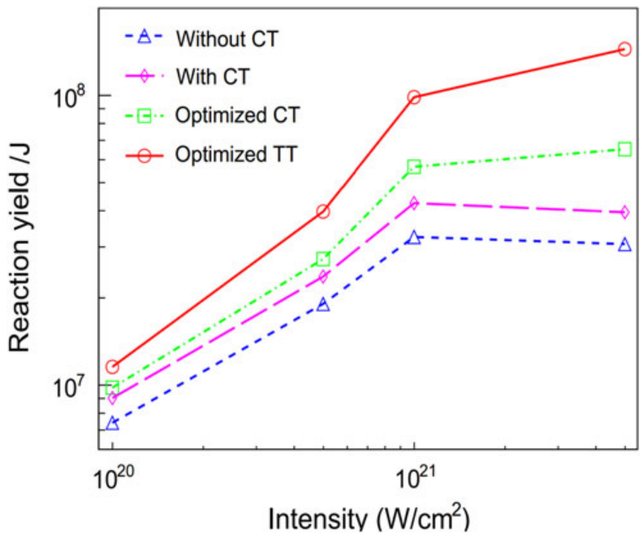

Fig. 10. The reaction yield at four different laser intensities. Without the CT, the target dimensions used in the simulations are $r_2 = 4$ and $T_2 = 3$ cm, and with CT they are $r_1 = 2$, $r_2 = 4$ cm, $T_1 = 0.5$ mm, and $T_2 = 3$ cm. With optimized CT, they are $r_1 = 2$, $r_2 = 4$, $T_2 = 3$ cm, and $T_1 = 1.0$, 1.5, 2.5, and 3.5 mm for the laser intensities 10^{20}, 5×10^{20}, 10^{21}, and 5×10^{21} W/cm^2, respectively. For the optimized CT and TT, they are $r_1 = 2$, $r_2 = 4$ cm, $T_1 = 1.0$, 1.5, 2.5, and 3.5 mm and $T_2 = 4$, 6, 8, and 10 cm.

optimized by the target geometry parameters. To illustrate these optimizations more clearly, the reaction yields for different cases of target geometry are shown in Figure 10. Clearly, with the CT the transmutation yield is enhanced. At laser intensities of $(1.0–5.0) \times 10^{20}$ W/cm^2 and 0.5 mm thick CT, the reaction yield is about 1.2–1.3 times that of without the CT. At the laser intensities 10^{20}, 5×10^{20}, 10^{21}, and 5×10^{21} W/cm^2, the recommended CT thicknesses are found to be 1.0, 1.5, 2.5, and 3.5 mm, respectively. The corresponding reaction yields are 1.1, 1.2, 1.3, and 1.7 times higher than that for the 0.5 mm convertor. The TT thicknesses were optimized further to 4, 6, 8, and 10 cm, and the corresponding reaction yields are 1.2, 1.5, 1.7, and 2.2 times higher compared with that for the 3 cm TT. Finally, the reaction yields are 0.1×10^8 J^{-1} for the 10^{20} W/cm^2 laser, 0.4×10^8 J^{-1} for the 5×10^{20} W/cm^2 laser, 1.0×10^8 J^{-1} for the 10^{21} W/cm^2 laser, and 1.4×10^8 J^{-1} for the 5×10^{21} W/cm^2 laser.

Figure 10 also shows that at laser intensities below 10^{21} W/cm^2, the reaction yield (per Joule of laser pulse energy) increases proportionally with the laser intensity, and at laser intensities exceeding 10^{21} W/cm^2, the reaction yield reaches saturation and decreases thereafter. This can be attributed to the fact that the normalization of reaction yield is by the laser pulse energy. There is thus an optimum laser intensity, namely 10^{21} W/cm^2, for maximum reaction yield. The corresponding reaction yield is about three times higher than that without the CT.

The laser repetition rate has direct effect on the yield, and attaining higher rates requires more advanced lasers. One can expect that 10^{21} W/cm^2 lasers with 1 kHz repetition rate can produce about 3.7×10^{11} reactions per second. The transmutation capability of intense laser-based electron source can therefore be comparable with that by photo-transmutation of long-lived radionuclides such as ^{135}Cs using Compton scattering classical γ-ray sources (Imasaki *et al*., 2006; Shuji *et al*., 2007; Zhu *et al*., 2016).

5. SUMMARY

In this paper, the possibility of photo-transmutation of long-lived radionuclide ^{135}Cs into the short-lived ^{134}Cs or the stable nuclide ^{133}Cs has been considered through Monte Carlo simulations. It is shown that the laser intensity and the geometry of both the convertor and the cesium target have strong influence on the reaction yield of ^{135}Cs. Moreover, proper choice of the target size for different laser intensities can enhance the transmutation efficiency by a factor of four. There is also an optimum laser intensity, namely 10^{21} W/cm^2, for producing maximum reaction yield. In view of the current advances in tabletop ultra-intense lasers, compact laser-based systems for photo-transmutation can be promising for nuclear waste management and medical isotope production.

ACKNOWLEDGMENTS

This work was supported by the National Natural Science Foundation of China (Grant Nos. 11405083 and 11347028) and the Research Foundation of Education Bureau of Hunan Province, China (Grant No. 14A120). W.L. appreciates the support from the Young Talent Project of the University of South China.

REFERENCES

Agostinelli, S., Allison, J., Amako, K., Apostolakis, J., Araujo, H., Arce, P., Asai, M., Axen, D., Banerjee, S., Barrand, G., Behner, F., Bellagamba, L., Boudreau, J., Broglia, L., Brunengo, A., Burkhardt, H., Chauvie, S., Chuma, J., Chytracek, R., Cooperman, G., Cosmo, G., Degtyarenko, P., Dell'acqua, A., Depaola, G., Dietrich, D., Enami, R., Feliciello, A., Ferguson, C., Fesefeldt, H., Folger, G., Foppiano, F., Forti, A., Garelli, S., Giani, S., Giannitrapani, R., Gibin, D. & Gómez Cadenas, J.J. (2003). Geant4-A simulation toolkit. *Nucl. Instrum. Methods A* **506**, 250–303.

Antici, P., Albertazzi, B., Audebert, P., Buffechoux, S., Hannachi, F., D'humières, E., Gobet, F., Grismayer, T., Mancic, A., Nakatsutsumi, M., Plaisir, C., Romagnani, L., Tarisien, M., Pépin, H., Sentoku, Y. & Fuchs, J. (2012). Measuring hot electron distributions in intense laser interaction with dense matter. *New J. Phys*. **14**, 063023.

Chen, C.D., Patel, P.K., Hey, D.S., Mackinnon, A.J., Key, M.H., Akli, K.U., Bartal, T., Beg, F.N., Chawla, S., Chen, H., Freeman, R.R., Higginson, D.P., Link, A., Ma, T.Y., MacPhee, A.G., Stephens, R.B., Van Woerkom, L.D., Westover, B. & Porkolab, M. (2009). Bremsstrahlung and K_α fluorescence measurements for inferring conversion efficiencies into fast ignition relevant hot electrons. *Phys. Plasmas* **16**, 082705.

Debayle, A., Honrubia, J.J., D'humières, E. & Tikhonchuk, V.T. (2010). Divergence of laser-driven relativistic electron beams. *Phys. Rev. E* **82**, 036405.

Esarey, E., Schroeder, C.B. & Leemans, W.P. (2009). Physics of laser-driven plasma-based electron accelerators. *Rev. Mod. Phys*. **81**, 1229–1285.

Galy, J., Hamilton, D.J. & Normand, C. (2009). High-intensity laser as radiation sources. *Eur. Phys. J., Spec. Top*. **175**, 147–152.

Galy, J., Maučec, M., Hamilton, D.J., Edwards, R. & Magill, J. (2007). Bremsstrahlung production with high-intensity laser matter interactions and applications. *New J. Phys*. **9**, 010023.

Giulietti, A., Bourgeois, N., Ceccotti, T., Davoine, X., Dobosz, S., D'oliveira, P., Galimberti, M., Galy, J., Gamucci, A., Giulietti, D., Gizzi, L.A., Hamilton, D.J., Lefebvre, E., Labate, L., Marquès, J.R., Monot, P., Popescu, H., Réau, F., Sarri, G., Tomassini, P. & Martin, P. (2008). Intense γ-ray source in the giant-dipole-resonance range driven by 10-TW laser pulses. *Phys. Rev. Lett*. **101**, 105002.

Glinec, Y., Faure, J., Le Dain, L., Darbon, S., Hosokai, T., Santos, J.J., Lefebvre, E., Rousseau, J.P., Burgy, F., Mercier, B. & Malka, V. (2005). High-resolution γ-ray radiography produced by a laser-plasma driven electron source. *Phys. Rev. Lett*. **94**, 025003.

Hanus, V., Drska, L., D'humieres, E. & Tikhonchuk, V. (2014). Numerical study of positron production with short-pulse high-intensity lasers. *Laser Part. Beams* **32**, 171–176.

Imasaki, K., Li, D., Miyamoto, S., Amano, S. & Mochizuki, T. (2006). High-brightness γ-Ray Generation for Nuclear Transmutation. *Lasers Nucl*. **694**, 147–167.

Irani, E., Sadighi, S.K., Zare, S. & Sadighi-Bonabi, R. (2012). Laser-induced photo transmutation of ^{126}Sn-A hazardous nuclear waste product-into short-lived nuclear medicine of ^{125}Sn. *Energy Convers. Manage*. **64**, 466–472.

Ledingham, K.W.D., Mckenna, P. & Singhal, R.P. (2003). Applications for nuclear phenomena generated by ultra-intense lasers. *Science* **300**, 1107–1111.

Luo, W., Zhu, Y.B., Zhuo, H.B., Ma, Y.Y., Song, Y.M., Zhu, Z.C., Wang, X.D., Li, X.H., Turcu, I.C.E. & Chen, M. (2015). Dense electron-positron plasmas and gamma-ray bursts generation by counter-propagating quantum electrodynamics-strong laser interaction with solid targets. *Phys. Plasmas* **22**, 063112.

Luo, W., Zhuo, H.B., Ma, Y.Y., Yang, X.H., Zhao, N. & Yu, M.Y. (2013). Ultrashort-pulse MeV positron beam generation from intense Compton-scattering γ-ray source driven by laser wakefield acceleration. *Laser Part. Beams* **31**, 89–94.

Magill, J., Schwoerer, H., Ewald, F., Galy, J., Schenkel, R. & Sauerbrey, R. (2003). Laser transmutation of iodine-129. *Appl. Phys. B* **77**, 387–390.

Mangles, S.P.D., Murphy, C.D., Najmudin, Z., Thomas, A.G.R., Collier, J.L., Dangor, A.E., Divall, E.J., Foster, P.S., Gallacher, J.G., Hooker, C.J., Jaroszynski, D.A., Langley, A.J., Mori, W.B., Norreys, P.A., Tsung, F.S., Viskup, R., Walton, B.R. & Krushelnick, K. (2004). Monoenergetic beams of relativistic electrons from intense laser–plasma interactions. *Nature* **431**, 535–538.

Moore, C.I., Knauer, J.P.K. & Meyerhofer, D.D. (1995). Observation of the transition from Thomson to compton scattering in multiphoton interactions with low-energy electrons. *Phys. Rev. Lett*. **74**, 2439–2442.

Quesnel, B. & Mora, P. (1998). Theory and simulation of the interaction of ultraintense laser pulse with electrons in vacuum. *Phys. Rev. E* **58**, 3719–3732.

Sadighi, S.K. & Sadighi-Bonabi, R. (2010). The evaluation of transmutation of hazardous nuclear waste of ^{90}Sr, into valuable nuclear medicine of ^{89}Sr by ultraintense lasers. *Laser Part. Beams* **28**, 269–276.

Sadighi-Bonabi, R., Irani, E., Safaie, B., Imani, K.H., Silatani, M. & Zare, S. (2010). Possibility of ultra-intense laser transmutation of ^{93}Zr(γ, *n*) ^{92} Zr a long-lived nuclear waste into a stable isotope. *Energy Convers. Manage*. **51**, 636–639.

Sadighi-Bonabi, R. & Kokabee, O. (2006). Evaluation of transmutation of ^{137}Cs(γ, *n*) ^{136}Cs using ultraintense lasers. *Chin. Phys. Lett*. **23**, 061434.

Schwoerer, H., Ewald, F., Sauerbrey, R., Galy, J., Magill, J., Rondinella, V., Schenkel, R. & Butz, T. (2003). Fission of actinides using a tabletop laser. *Europhys. Lett*. **61**, 47–52.

Schwoerer, H., Pfotenhauer, S., Jäckel, O., Amthor, K.-U., Liesfeld, B., Ziegler, W., Sauerbrey, R., Ledingham, K.W.D. & Esirkepov, T. (2006). Laser-plasma acceleration of quasi-monoenergetic protons from microstructured targets. *Nature* **439**, 445–448.

Sentoku, Y., Bychenkov, V.Y., Flippo, K., Maksimchuk, A., Mima, K., Mourou, G., Sheng, Z.M. & Umstadter, D. (2002). High-energy ion generation in interaction of short laser pulse with high-density plasma. *Appl. Phys. B* **74**, 207–215.

Shkolnikov, P.L., Kaplan, A.E., Pukhov, A. & Meyer-Ter-vehn, J. (1997). Positron and gamma-photon production and nuclear reactions in cascade processes initiated by a sub-terawatt femtosecond laser. *Appl. Phys. Lett*. **71**, 3471–3473.

Shuji, M., Yoshihiro, A., Sho, A., Dazhi, L., Kazuo, I., Hiroaki, K., Yoshihiko, S., Tetsuya, T. & Takayasu, M. (2007). Laser Compton back-scattering gamma-ray beamline on NewSUBARU. *Radiat. Meas*. **41**, 179–185.

Takashima, R., Hassegawa, S., Nemoto, K. & Kato, K. (2005). Possibility of transmutation of ^{135}Cs by ultraintense laser. *Appl. Phys. Lett*. **86**, 011501.

Tanimoto, T., Habara, H., Kodama, R., Nakatsutsumi, M., Tanaka, K.A., Lancaster, K.L., Green, J.S., Scott, R.H.H., Sherlock, M., Norreys, P.A., Evans, R.G., Haines, M.G., Kar, S., Zepf, M., King, J., Ma, T., Wei, M.S., Yabuuchi, T., Beg, F.N., Key, M.H., Nilson, P., Stephens, R.B., Azechi, H., Nagai, K., Norimatsu, T., Takeda, K., Valente, J. & Davies, J.R. (2009). Measurements of fast electron scaling generated by petawatt laser systems. *Phys. Plasmas* **16**, 062703.

Wilks, S.C., Krurer, W.L., Tabak, M., & Langdon, A.B. (1992). Absorption of ultra-intense laser pulses. *Phys. Rev. Lett*. **69**, 1383–1386.

Yan, Y.H., Zhao, Z.Q., Wu, Y.C., Gu, Y.Q., Cao, L.F., Yao, Z.E., Teng, J., Dong, K.G., Liu, D.X., Fan, W., Wei, L. & Yu, J.Q. (2012). Monte Carlo simulation study of positron generation in ultra-intense laser-solid interactions. *Phys. Plasmas* **19**, 023114.

Yang, W.S., Kim, Y., Hill, R.N., Taiwo, T.A. & Khalil, H.S. (2004). Long-lived fission product transmutation studies. *Nucl. Sci. Eng*. **146**, 291–318.

Zhu, Z.C., Luo, W., Li, Z.C., Song, Y.M., Wang, X.D., Wang, X.L. & Fan, G.T. (2016). Photo-transmutation of long-lived nuclear waste ^{135}Cs by intense Compton γ-ray source. *Ann. Nucl. Energy* **89**, 109–114.